ARTICLE

Theoretical Study on Mechanism of Reaction of OH with HO_2NO_2

Yan Tian[a,c], Tian-jing He[a*], Li He[b], Fan-chen Liu[a], Dong-ming Chen[a]

a. Department of Chemical Physics, University of Science and Technology of China, Hefei 230026, China;
b. Department of Electronic Science and Technology, University of Science and Technology of China, Hefei 230026, China;
c. School of Science, Anhui Agricultural University, Hefei 230036, China

(Dated: Received on January 24, 2007; Accepted on March 26, 2007)

The reaction of HO_2NO_2 (peroxynitric acid, PNA) with OH was studied by the hybrid density functional B3LYP and CBS-QB3 methods. Based on the calculated potential energy surface, five reaction channels, H_2O+NO_2+O_2, HOOH+NO_3, NO_2+HO_3H, HO_2+$HONO_2$ and HO_2+HOONO, were examined in detail. The major reaction channel is PNA+OH→M1→TS1→H_2O+NO_2+O_2. Taking a pre-equilibrium approximation and using the CBS-QB3 energies, the theoretical rate constant of this channel was calculated as 1.13×10^{-12} cm^3/(molecule s) at 300 K, in agreement with the experimental result. Comparison between reactions of $HOONO_2$+OH and $HONO_2$+OH was carried out. For HOR+OH reactions, the total rate constants increase from R=NO_2 to R=ONO_2, which is consistent with experimental measurements.

Key words: Reaction, Peroxynitric acid, *ab initio* calculation, Rate constant

I. INTRODUCTION

HO_2NO_2 (peroxynitric acid, PNA) is formed in the atmosphere by the association reaction of HO_2 with NO_2. As early as 1977, Nike *et al.* verified that HO_2NO_2 was a molecule, and not a simple complex, by using IR spectrum [1]. After that there have been considerable efforts in the study of the formation and loss processes of PNA, including the preparation, decomposition photochemistry and pulse radiolysis.

It has been confirmed that the PNA molecule plays an important role in the Earth's upper troposphere and lower stratosphere (UTLS) as a reservoir for both HO_x (OH and HO_2) and NO_x (NO and NO_2) species [2-3]. Besides, the product of the reaction of OH with PNA is a significant sink for HO_x in the lower stratosphere (LS). As a result, PNA plays an important role in determining ozone abundance and its changes over time in the lower stratosphere [4-8].

The dominant atmospheric loss processes for HO_2NO_2 consist of thermal decomposition [9], photodissociation (UV and Visible/near-IR) [10], and reaction with the OH radical.

$$HO_2NO_2 + M \rightarrow HO_2 + NO_2 + M \quad (1)$$

$$HO_2NO_2 + h\nu \rightarrow \text{Products} \quad (2)$$

$$HO_2NO_2 + OH \rightarrow \text{Products} \quad (3)$$

Each of these loss processes may have different impacts in the UTLS, in terms of the partitioning and removal of HO_x and NO_x. Thermal decomposition, near-infrared photodissociation processes and overtone absorption do not remove OH, HO_x and NO_x from the atmosphere [10]. However, UV photolysis and the reaction of HO_2NO_2 with OH may contribute to the loss of the reactive HO_x and NO_x radicals, depending on the products of these two processes.

The rate constant for reaction (3) has been previously measured in the laboratory by using both absolute [11,12] and relative [13] kinetic methods. The room temperature values of k_3 reported in these studies ranged from 2.4×10^{-12} cm^3/(molecule s) to 6.2×10^{-12} cm^3/(molecule s) [4,11-13]. Such differences are not surprising due to the difficulties in determining the PNA concentration and accounting for the influence of reactive impurities. In addition, the unambiguous mechanism of reaction (3) is still not clear.

In this work, a high level of theory is employed to study the mechanism of the reaction of OH+PNA. The information on the potential energy surface (PES) is directly obtained from *ab initio* calculations. Such investigation can provide useful information for chemical-dynamic analysis.

II. COMPUTATIONAL METHODS

All of the electronic structure calculations in our present study were carried out with the Gaussian 03 program [14]. The geometries of the reactants, products, intermediates, and transition states of the reaction HO_2NO_2+OH were fully optimized by using the hybrid density functional B3LYP method with the CBSB7(6-311G(2d,d,p)) basis set. Vibrational frequencies were calculated at the same level to determine the nature and zero-point energy (ZPE) corrections of the stationary points. Each saddle point was verified to connect the proper reactants and products by performing an in-

*Author to whom correspondence should be addressed. E-mail: tj16@ustc.edu.cn, Fax: +86-551-3603388

trinsic reaction coordinate (IRC [15]) calculation. The single point energy calculations for all species were performed at the multilevel techniques based on additive energy corrections of CBS-QB3 [16]. In this work, additional calculations were carried out in some cases using G3B3 method to confirm the energies obtained by the CBS-QB3 method. Unless otherwise specified, the CBS-QB3 single-point energies are used in the following discussions.

III. RESULTS AND DISCUSSION

The optimized geometries of stationary points are shown in Fig.1. The overall energy profile based on the CBS-QB3 method is depicted in Fig.2. The vibrational frequencies including available experimental data for PNA are summarized in Table I and the scaled harmonic vibrational frequencies of the main stationary points are listed in Table II.

A. Structure and vibrational frequencies of PNA

Some theoretical studies have been performed to investigate pernitric acid [17-20]. Chen and Hamilton showed that a minimum structure calculated with the B3LYP method was similar to that calculated with both MP2 and QCISD methods using similar size basis sets [18]. Aloisio *et al.* obtained the geometry of PNA using the B3LYP method [20], which is in line with the structure calculated by Chen and Hamilton. Meanwhile, Jitariu *et al.* achieved three rotational isomers for PNA at different levels of theory and their calculations also indicated that the three isomers have the same energy at the G2MP2 level of theory [19]. More recently, Matthews and Sinha studied the structure and vibrational spectra of HO_2NO_2 using a high-level *ab initio* method [21]. They revealed that there was a significant basis set dependence in the predicted *ab initio* structure for PNA, and the calculations with the smaller basis set may not provide an accurate representation of the experimental geometry for PNA. Based on these results, the basis set 6-311++G(2df,2p) was employed to calculate the geometry of PNA in this work. The singlet geometries of PNA obtained in these calculations with two different basis sets are given in Fig.1. The global minimum structure is in good agreement with that calculated by Saxon *et al.* [17] and Jitariu *et al.* [19], having no symmetry and the plane of the HO_2 group roughly perpendicular to the plane of the NO_2 group. The dihedral angles of HOON are 87.3° and 88.0° with the CBSB7 and 6-311++G(2df,2p) basis sets, respectively, which are in line with 85.9° at the CCSD(T)/aug-cc-pVTZ level [21].

Frequencies and IR intensities calculated for PNA in the present work are given in Table I along with the observed values [22-24]. From Table I it can be seen that all of the MP2 calculations of Chen *et al.* [18] and Jitariu *et al.* [19] and the CCSD(T) calculations of Matthews *et al.* [21] overestimated the higher frequencies. The unscaled frequencies here based on B3LYP calculations are in line with their results. In contrast, in Table II, it is very clear that the scaled frequencies (scale factor is 0.96) of PNA in these calculations are in good agreement with the available experimental values. At the B3LYP/CBSB7 level the rotational constants A=12.039, B=4.613, C=3.375 GHz were also generated; they are in good agreement with the experimental values (A=11.994, B=4.665, C=3.397 GHz) [24]. The results indicate the method used in this work is appropriate.

B. Channels for HO_2NO_2+OH reactions

In these calculations there are five channels to produce five products, H_2O+NO_2+O_2 (P1), HOOH+NO_3 (P2), NO_2+HO_3H (P3), HO_2+$HONO_2$ (P4), and HO_2+HOONO (P5), and four intermediate complexes, $HOHOONO_2$ (M1), $(HOO)_2NO$ (M2), $HOON(O)_2OH$ (M3a and M3b).

$$\mathrm{PNA + OH \rightarrow M1 \rightarrow TS1 \rightarrow P1} \tag{4}$$

A pre-reaction hydrogen-bonded complex M1 ($O_2NOOHOH$) is formed due to the dipole-dipole interaction between the oxygen atom of the OH radical and the hydrogen atom of PNA, as illustrated in Fig.1. The forming HO$\cdots$H bond is 1.894 Å in M1, which is in the range of hydrogen bond length 1.7-2.3 Å, while the O5−H6 bond is elongated to 0.982 Å. The dihedral angle of NOOH is reduced to 81.3°, and the formation of HOH angle is 92.5°. The relative energies calculated at the CBS-QB3 and G3B3 levels of theory for M1 are −19.2 and −18.8 kJ/mol, respectively.

M1 can decompose to P1 via a transition state TS1. This is an N2−O4 and O5−H6 scission and O−H6 formation process. The breaking N2−O4 and O5−H6 bonds in TS1 are elongated to 1.546 and 1.022 Å, respectively. Meanwhile, the forming O−H6 bond is shortened to 1.468 Å. At the same time the angle of ∠HOH6 increases to 110.3°, tending to form an H_2O molecule. Energetically, TS1 is located at 1.2 kJ/mol above the reactants, while the relative energy calculated at the G3B3 level for TS1 is 14.6 kJ/mol. Considering the different levels of theory, such differences are reasonable. The relative energy of product P1 is −193.9 kJ/mol.

$$\mathrm{PNA + OH \rightarrow TS2 \rightarrow P2} \tag{5}$$

The oxygen atom of OH radical can attack one of the oxygen atoms of PNA to form the product P2. With the approaching of O7 and O5 and the stretching of O4−O5, the transition state TS2 is reached. In TS2 the forming O5−O7 bond is shortened to 1.793 Å while the

DOI:10.1088/1674-0068/21/01/32-38

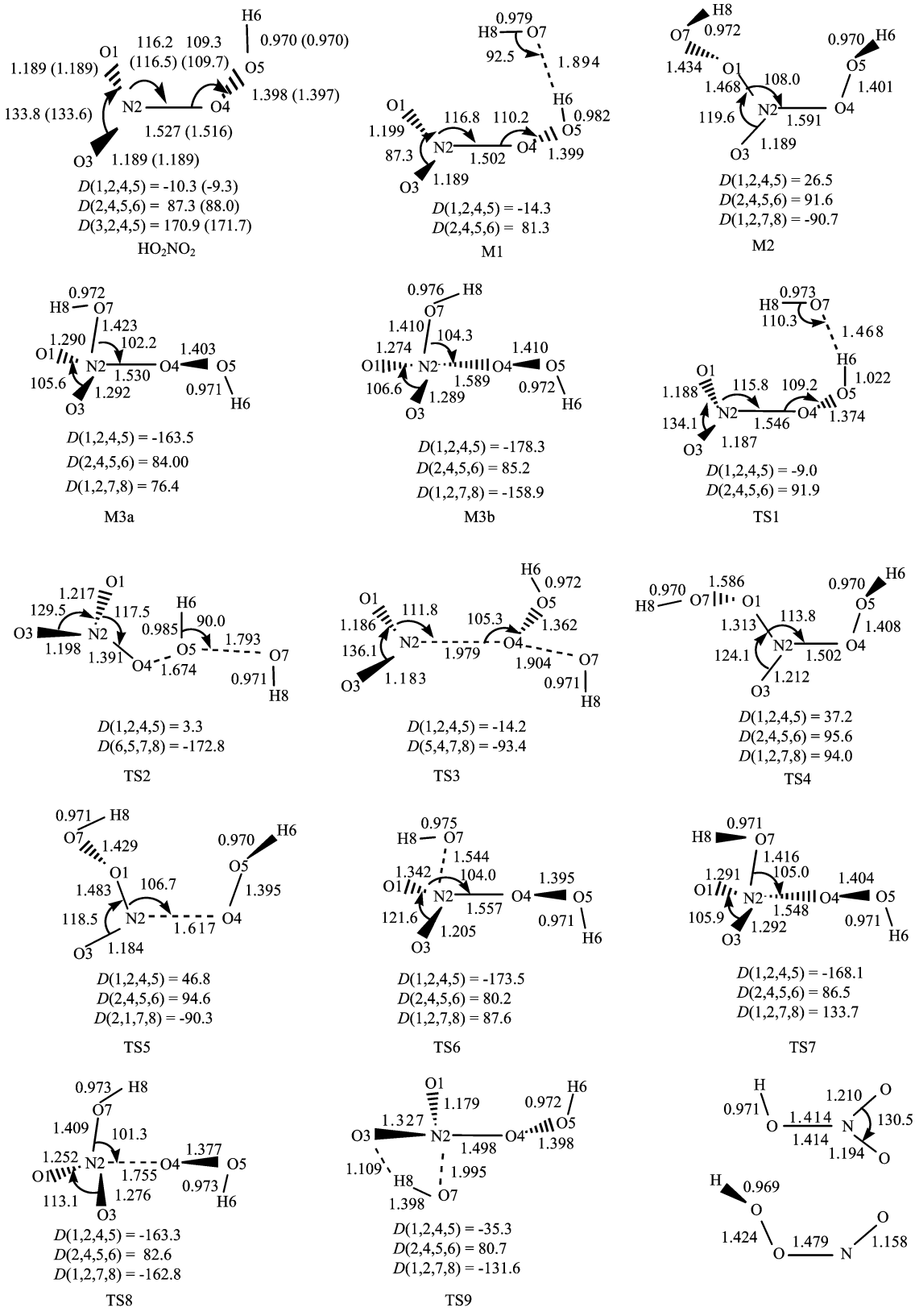

FIG. 1 Optimized structures of various species involved in the reaction of HO_2NO_2 with OH at the B3LYP/6-311G(2d, d, p) level, the values in parentheses were calculated using the 6-311++G(2df,2p) basis set. Bond distances are in Å and angles are in (°).

DOI:10.1088/1674-0068/21/01/32-38

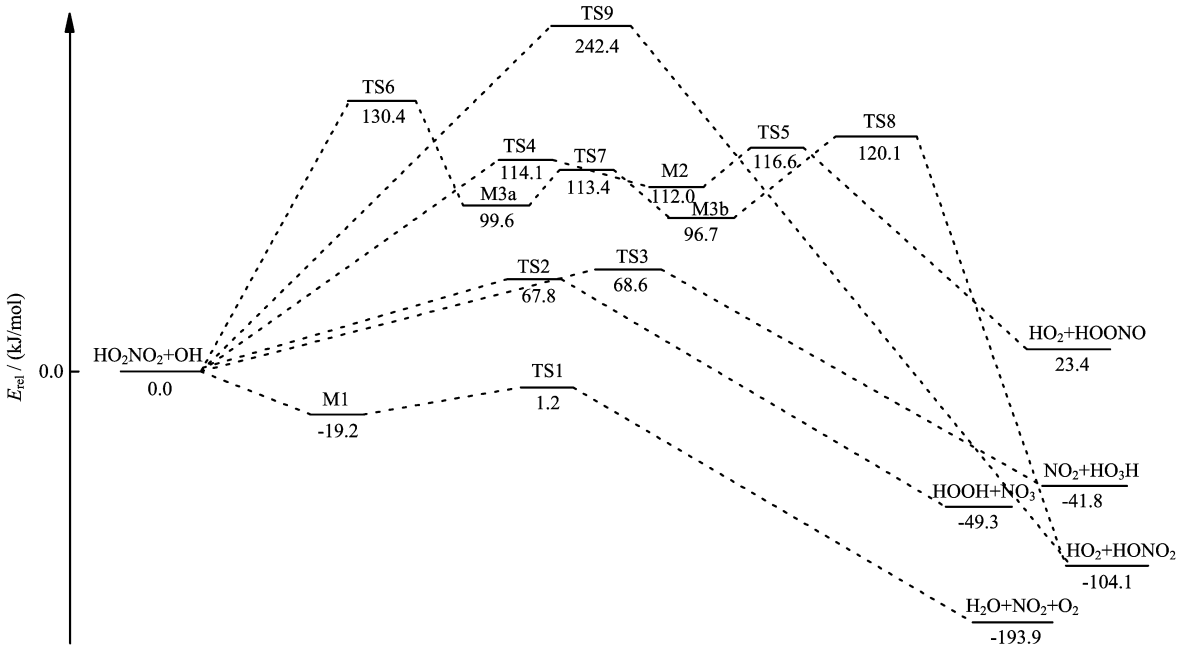

FIG. 2 The overall profile of the potential energy surface for the reaction of OH with HO_2NO_2, calculated at the CBS-QB3 level.

TABLE I Vibrational frequencies (cm^{-1}) and assignments for HO_2NO_2

SCF [17]	MP2 [18]	MP2 [20]		B3LYP[a]		CCSD(T) [21]	Obsd.	Mode
		Freq.	Rel.	Freq.	Rel.			
4100	3804	3791	52	3719(3718)	48	3728	3540 [22]	OH str
1960	1942	1951	254	1822(1788)	394	1821	1728 [22]	O1NO3 asym str
1615	1445	1410	54	1431(1437)	59	1426	1397 [22]	OOH bend
1576	1326	1324	200	1365(1348)	240	1355	1304 [22]	O1NO3 sym str
1215	994	973	46	995(999)	43	929	945 [23]	O−O str
1046	795	786	143	822(814)	117	807	803 [22]	O1NO3 sciss
896	753	721	6	738(747)	13	727	722 [23]	O1NO3 umbrella
821	669	645	37	657(660)	11	640	654 [23]	O1NO4 bend
652	457	410	89	454(460)	20	450	483 [23]	NO4 str
436	378	356	61	377(370)	76	370	340 [23]	HOO bend
302	320	302	19	304(305)	18	299	–	HOO tor
145	152	119	15	148(148)	12	132	145 [24]	O−NO−O tor

[a] Unscaled frequencies calculated in this work, the values in parentheses were calculated using the 6-311++G(2df,2p) basis set.

breaking O4−O5 bond is elongated to 1.674 Å. From Fig.1 we can also see that the N−O4 bond is shortened to 1.391 Å. The relative energies of TS2 and P2 are 67.7 and −49.3 kJ/mol, respectively, while the calculated energy of TS2 at the G3B3 level is 76.5 kJ/mol.

$$\mathrm{PNA} + \mathrm{OH} \rightarrow \mathrm{TS3} \rightarrow \mathrm{P3} \qquad (6)$$

Besides the O5 atom, the O4 atom of the PNA molecule can also be attacked by the O atom of the OH radical. This is a direct reaction process via a transition state TS3 with a barrier of 68.6 kJ/mol. This indicates that TS3 and TS2 have nearly the same energy at the CBS-QB3 level. From Fig.1 we can see that the forming O4−O7 bond in TS3 is shortened to 1.904 Å while the breaking N2−O4 bond is elongated to 1.979 Å. The relative energy of P3 is −41.8 kJ/mol.

Since the P3 product has not been detected in past experimental research, this reaction channel was also calculated using the G3B3 method. The relative energy of TS3 was determined to be 83.2 kJ/mol. From above results we can see that at the G3B3 level the relative energy of TS3 is only 6.7 kJ/mol higher than that of

DOI:10.1088/1674-0068/21/01/32-38

TABLE II Vibrational frequencies of species for the PNA+OH reaction at the B3LYP/CBSB7 level of theory

Species	Frequencies/cm^{-1}
PNA	143, 292, 362, 436, 630, 708, 789, 955, 1310, 1374, 1749, 3571
OH	3557
M1	64, 107, 147, 207, 226, 317, 351, 448, 607, 674, 735, 793, 960, 1301, 1440, 1719, 3373, 3512
M2	56, 96, 195, 234, 303, 341, 403, 457, 561, 676, 729, 847, 942, 1337, 1355, 1483, 3553, 3581
M3a	111, 225, 248, 357, 385, 450, 475, 539, 635, 656, 829, 847, 939, 1102, 1372, 1386, 3562, 3577
M3b	93, 248, 340, 361, 403, 452, 513, 552, 622, 688, 808, 832, 923, 1140, 1346, 1381, 3501, 3558
TS1	361i, 58, 76, 184, 216, 304, 381, 446, 598, 632, 715, 778, 991, 1298, 1383, 1754, 2371, 3588
TS2	689i, 76, 120, 238, 241, 354, 396, 592, 609, 703, 733, 854, 893, 1207, 1283, 1639, 3371, 3613
TS3	423i, 48, 103, 127, 187, 202, 234, 351, 373, 512, 737, 752, 951, 1326, 1383, 1743, 3542, 3608
TS4	567i, 70, 119, 237, 267, 280, 371, 421, 589, 620, 755, 876, 965, 1158, 1362, 1434, 3572, 3602
TS5	147i, 44, 145, 225, 263, 298, 374, 399, 532, 634, 736, 858, 946, 1341, 1358, 1507, 3570, 3575
TS6	289i, 104, 261, 301, 372, 383, 438, 463, 550, 634, 672, 901, 946, 1201, 1384, 1422, 3564, 3594
TS7	263i, 114, 244, 370, 383, 455, 473, 540, 626, 678, 831, 849, 936, 1126, 1332, 1377, 3563, 3589
TS8	1264i, 87, 229, 250, 338, 355, 446, 485, 567, 583, 804, 826, 957, 1073, 1320, 1362, 3531, 3555
TS9	1338i, 104, 199, 245, 276, 368, 384, 556, 613, 682, 784, 835, 942, 1131, 1388, 1602, 2063, 3555

TS2, and there is only a 0.8 kJ/mol difference between TS2 and TS3 at the CBS-QB3 level. Thus we conclude that the channel of the formation of the P3 product is also feasible. Based on these results, future experimental studies are strongly desired to confirm this channel.

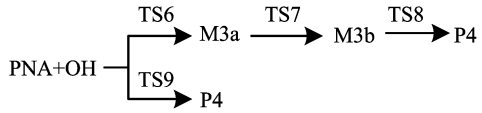

It is very interesting that P4 can be formed through two different pathways. One is a direct reaction via a four-membered ring transition state TS9 with a barrier of 242.4 kJ/mol. The other is a consecutive reaction process. Firstly, the O atom of the OH radical is added to the N atom of the PNA molecule via a transition state TS6 with the formation of the complex M3a. The corresponding barrier is 130.4 kJ/mol. Then M3a isomerizes to M3b via an H−ON rotational transition state TS7. Finally, M3b decomposes to the final product P4 via an N2−O4 breaking transition state TS8. The relative energies of M3a, TS7, M3b, TS8, and P4 are 99.5, 113.3, 96.6, 120.0, and −104.1 kJ/mol, respectively. Owing to the higher barrier for the two processes, they do not play an important role in the overall reaction.

$$\mathrm{PNA + OH \rightarrow TS4 \rightarrow M2 \rightarrow TS5 \rightarrow P5} \qquad (7)$$

here is another channel that can produce the HO_2 radical. The PNA and OH radical may approach each other through the O atom of the OH radical and the O1 atom of the PNA molecule to form a complex M2 via a transition state TS4. With the gradual approach of the O atom of the OH radical to the O1 atom of the PNA molecule and the stretching of the N2−O1 bond, the TS4 structure occurs. In TS4 the forming O7−O1 bond is 1.586 Å and it is shortened to 1.434 Å in M2, while the N2−O1 bond is elongated to 1.313 Å in TS4 and it is only stretched by 0.155 Å in M2. As shown in Fig.2, M2 can further decompose to HO_2 and HOONO via an N−O breaking transition state TS5 with a small barrier of 4.6 kJ/mol. The breaking N2−O4 bond in TS5 is elongated to 1.617 Å, while the O4−O5 bond is only slightly shortened by 0.006 Å. The calculated relative energies of TS4, M2, TS5, and P5 are 114.1, 112.0, 116.6, and 23.4 kJ/mol, respectively. This pathway has been confirmed by IRC calculations. Note that the barrier is so high that this process does not easily occur at room temperature.

The schematic description of the PES of the reaction is shown in Fig.2. Indeed, P1 is a preferable product in view of thermodynamics because it has the lowest energy among the five products. Since it has the lowest barrier, taking kinetics into account, P1 is still the dominant product. As a result, we believe that H_2O+NO_2+O_2 is the main product for the title reaction and this is in good agreement with the experimental observations [4,11-13]. In view of kinetics, we can see that the channel of formation for product P3 is also a feasible pathway, which is not in line with the conclusions by Jiménez *et al.* [4]. Jiménez *et al.* studied the reaction of PNA+OH by producing OH via pulsed laser photolysis (PLP) and detecting OH via laser-induced fluorescence (LIF). They also reported the first experimental determination of the product branching ratios for reaction (3). They concluded that the branching ratios for the production of P2 and P4 at 298 K were <5% and <10%, respectively, and H_2O+NO_2+O_2 (P1) were the dominant products. The product P3 was not reported in their work.

In addition, the enthalpy changes ΔH°_{298} between the

DOI:10.1088/1674-0068/21/01/32-38

reactants and products for the reaction of PNA+OH at CBS-QB3 level are also calculated. The ΔH°_{298} of the P1 pathway is −188.9 kJ/mol at the CBS-QB3 level, which is in good agreement with the JPL 02-25 value of −191.4 kJ/mol [25]. For the P2 and P4 channels, the ΔH°_{298} between the reactants and the products are −49.3 and −106.2 kJ/mol, respectively, which are also in line with the JPL values of −46.4 and −104.1 kJ/mol [25], respectively. However, for the channels of products P3 and P5 there are no comparable experimental values. The calculated ΔH°_{298} values in this work are −43.1 and 23.8 kJ/mol, respectively. As a result, in view of thermodynamics the channels of products P3 and P5 do not play important roles in the overall reaction.

Moreover, the theoretical rate constant of product P1 pathway was calculated using the CBS-QB3 energies. In 2001, Alvarez-Idaboy *et al.* studied the reactions of OH with CH_2O and CH_3CH_2O [26]. They proposed that the reaction occurs according to the following two-step mechanism

$$\text{Step1}: \quad \mathrm{RHC{=}O + OH \leftrightarrow [RHC{=}O\cdots HO\cdot]} \quad (8)$$

$$\text{Step2}: \quad \mathrm{[RHC{=}O\cdots HO\cdot] \rightarrow RC{=}O\cdot + H_2O} \quad (9)$$

They believed the reaction involved a fast pre-equilibrium between the reactants and the prereactive complex followed by an internal rearrangement leading to the elimination of a water molecule. If k_f and k_r are the rate constants for the forward and reverse reactions of the first step, respectively, and k_b is the rate constant for the second step, then the rate constant for the overall reaction can be written as

$$k = \frac{k_f k_b}{k_r} = \frac{A_f A_b}{A_r} \exp\left(-\frac{E_f + E_b - E_r}{RT}\right) \quad (10)$$

In this reaction, the energy difference between the barrier E_r and E_b is only 0.12 kJ/mol. However, the entropy change in the reverse reaction of the first step reaction is larger than that in the formation of the products of the second step reaction. Thus, one can expect k_r to be considerably larger than k_b [27]. Based on this assumption, they obtained a reliable result [26]. For the reverse process of M1 formation in OH+PNA reactions, the variation transition state theory (VTST) was used in the current work to obtain the value of k_r, which is truly higher than k_b. As a result, for this complex consecutive process: PNA+OH↔M1→P1, the same method was used as Alvarez-Idaboy *et al.* used in Ref.[26] to calculate the rate constant. The calculated rate constant is 1.13×10^{-12} cm^3/(molecule s) at 300 K. The experimental result was 3.42×10^{-12} cm^3/(molecule s) [4].

C. Comparison with the HNO_3+OH reaction

The dominant loss of HO_x in the lower stratosphere is due to the reactions of the hydroxyl radical with peroxynitric acid (HO_2NO_2) and with nitric acids ($HONO_2$ or HNO_3) [28]. Thus it is very meaningful to compare the PES feature of the reaction of HO_2NO_2+OH with that of the analogous reaction $HONO_2$+OH.

In 2000, Xia *et al.* studied the mechanism of the OH+$HONO_2$ reaction by *ab initio* molecular orbital calculations at the G2M(cc3) level of theory [29]. They reported four different reaction channels including four complexes and four transition states. The possible reaction pathways are summarized as

$$\begin{aligned} \mathrm{OH + HONO_2} &\rightarrow \mathrm{LM1 \rightarrow TS1 \rightarrow H_2O + NO_3} \\ &\rightarrow \mathrm{LM2 \rightarrow TS2 \rightarrow H_2O + NO_3} \\ &\rightarrow \mathrm{LM3a \rightarrow TS3 \rightarrow LM3b} \\ &\rightarrow \mathrm{TS4 \rightarrow H_2O_2{+}NO_2} \end{aligned} \quad (11)$$

By comparing the theoretical results, we find that both reactions involve the same initial association process, that is, the oxygen-to-hydrogen process, HOR+OH→HO·HOR (R=ONO_2, NO_2), to form a molecular complex through hydrogen bonding with no barrier. Xia *et al.* reported two different structures of HO·$HONO_2$, and they both dissociate to the products H_2O and NO_3. In their work the calculated hydrogen bond lengths ranged from 1.683 Å to 1.817 Å, which are slightly shorter than that of the HO·$HOONO_2$ system (1.894 Å). From the PES of these two different systems, we can see that the pathway of the complex HO·HOR (R=ONO_2, NO_2) decomposition to the final products is the main reaction channel in their reaction systems. Both of them have the lowest energy barriers. In the HO+$HONO_2$ system, the barrier height is 27.6 kJ/mol at the G2M(cc3) level.

In order to study the relation between the structure and properties for the analogous reactions and find a proper method to study the kinetic behavior for the reaction of HO_2NO_2+OH, the OH+$HONO_2$→LM2→TS2→H_2O+NO_3 pathway was also calculated using the CBS-QB3 method. The results indicate that the optimized geometries of LM2 and TS2 at the B3LYP/CBSB7 level of theory are in good agreement with those reported by Xia *et al.* [29]. The relative energies of LM2 and TS2 were calculated as −19.6 and 6.7 kJ/mol at the CBS-QB3 level, respectively. These values are also consistent with those obtained by Xia *et al.* [29]. The dissociation energy of LM2 is about 26.3 kJ/mol, which is a little higher than that of the HO+$HOONO_2$ system (20.5 kJ/mol). This difference was probably caused by NO_3 radicals with higher electronegativity than that of NO_2 radicals, which strongly attracts the electrons located on the OH radical. Thus, theoretically, the hydrogen atom in the PNA molecule has more positive charges than that in the $HONO_2$ molecule.

For these two reactions, it is obvious that they both have the reaction channel that forms the HOOH molecule. Meanwhile, as discussed above, the NO_3 radicals have higher electronegativity than that of the NO_2 radicals, which leads to the O−O bond rupture of the

DOI:10.1088/1674-0068/21/01/32-38

PNA molecule being easier than the N−O bond cleavage of the $HONO_2$ molecule. At the CBS-QB3 level the O−O bond energy of PNA is 158.4 kJ/mol, while the N−O(H) bond energy of $HONO_2$ is 201.9 kJ/mol. Furthermore, based on the PES, the energy barriers are 67.7 kJ/mol for the O−O bond rupture in the PNA+OH reaction and 102.0 kJ/mol for the N−O bond fission in the OH+$HONO_2$ reaction, respectively. These theoretical predictions are in agreement with the experimental results. The experimental rate constants of HOR with OH radical (298 K) are $(6.2\pm0.4)\times10^{-12}$ cm^3/(molecule s) for R=NO_3 [12] and $(1.4\pm0.2)\times10^{-13}$ cm^3/(molecule s) for R=NO_2 [12], respectively.

It should be pointed out that in the reaction system of OH+PNA, there also is an N−O bond cleavage reaction pathway with a barrier of 68.6 kJ/mol, which is competitive with the O−O fission reaction channel. Moreover, three adduct complexes M2, M3a, and M3b also formed for the reaction of OH+PNA, while only two other hydrogen bonding complexes LM3a and LM3b were obtained in the OH+$HONO_2$ system.

IV. CONCLUSION

The hybrid density functional B3LYP method, G3B3 method and CBS-QB3 method were used to investigate the PES for the reaction of HO_2NO_2(PNA) with OH. Four intermediate complexes, nine transition states and five product channels, H_2O+NO_2+O_2 (P1), HOOH+NO_3 (P2), NO_2+HO_3H (P3), HO_2+$HONO_2$ (P4) and HO_2+HOONO (P5), were examined in detail. Based on the PES, the major reaction channel is PNA+OH→M1→TS1→P1, via a very lower barrier height. Based on the pre-equilibrium approximation between the reactants and the prereactive complex, the theoretical rate constant of product P1 pathway is calculated by using the CBS-QB3 energies. The calculated rate constant is 1.13×10^{-12} cm^3/(molecule s) at 300 K, which is in agreement with the experimental result (3.42×10^{-12} cm^3/(molecule s)). A comparison of the $HOONO_2$+OH reaction with the analogous reaction of $HONO_2$+OH was carried out. For the HOR+OH reactions, the total rate constants increase from R=NO_2 to R=ONO_2, which is consistent with the experimental measurements.

V. ACKNOWLEDGMENT

This work was supported by the National Natural Science Foundation of China (No.20473078).

[1] H. Niki, P. D. Maker, C. M. Savage, and L. P. Breitenbach, Chem. Phys. Lett. **45**, 564 (1977).
[2] J. H. Seinfeld and N. S. Pandis, *Atmospheric Chemistry and Physics*, New York: Wiley, (1998).
[3] *WMO/UNEP Scientific Assessment of Ozone Depletion*, Geneva, Switzerland: National Aeronautics and Space Administration, (1998).
[4] E. Jiménez, T. Gierczak, H. Stark, J. B. Burkholder, and A. R. Ravishankara, J. Phys. Chem. A **108**, 1139 (2004).
[5] W. M. Wei, W. Tan, T. J. He, D. M. Chen, and F. C. Liu, Chin. J. Chem. Phys. **17**, 679 (2004).
[6] L. C. Li, H. P. Zhou, and Z. H. Tang, Chin. J. Chem. Phys. **14**, 47 (2001).
[7] T. J. He, D. M. Chen, F. C. Liu, and L. S. Sheng, Chem. Phys. Lett. **332**, 545 (2000).
[8] Y. Tian, W. M. Wei, Z. M. Tian, H. Y. Yang, T. J. He, D. M. Chen, and F. C. Liu, J. Phys. Chem. A **110**, 11145 (2006).
[9] T. Gierczak, E. Jiménez, V. Riffault, J. B. Burkholder, and A. R. Ravishankara, J. Phys. Chem. A **109**, 586 (2005).
[10] C. M. Roehl, S. A. Nizkorodov, H. Zhang, G. A. Blake, P. O. Wennberg, J. Phys. Chem. A **106**, 3766 (2002).
[11] P. L. Trevor, G. Black, and J. R. Barker, J. Phys. Chem. **86**, 1661 (1982).
[12] C. A. Smith, L. T. Molina, J. J. Lamb, and M. J. Molina, J. Int. J. Chem. Kinet. **16**, 41 (1984).
[13] I. Barnes, V. Bastian, K. H. Becker, E. H. Fink, and F. Zabel, Chem. Phys. Lett. **123**, 28 (1986).
[14] M. J. Frisch, G. W. Trucks, H. B. Schlegel, *et al.*, *GAUSSIAN 03, Revision B.04*, Pittsburgh, PA, Gaussian, Inc., (2003).
[15] C. Gonzalez and H. B. Schlegel, J. Chem. Phys. **90**, 2154 (1989).
[16] J. A. Montgomery, Jr., M. J. Frisch, J. W. Ochterski, G. A. Petersson, J. Chem. Phys. **110**, 2822 (1999).
[17] R. P. Saxon and B. Liu, J. Phys. Chem. **89**, 1227 (1985).
[18] Z. Chen and T. P. Hamilton, J. Phys. Chem. **100**, 15731 (1996).
[19] L. C. Jitariu and D. M. Hirst, J. Phys. Chem. A **103**, 6673 (1999).
[20] S. Aloisio and J. S. Francisco, J. Phys. Chem. A **104**, 6212 (2000).
[21] J. Matthews, A. Sinha, and J. S. Francisco, J. Chem. Phys. **12**, 5720 (2004).
[22] H. Niki, P. D. Marker, C. M. Savage, and L. P. Breitenbach, Chem. Phys. Lett. **45**, 564 (1977).
[23] E. H. Appelman and D. J. Gosztola, Inorg. Chem. **34**, 787 (1995).
[24] R. D. Suenram, F. J. Lovas, and H. M. J. Pickett, Mol. Spectrosc. **116**, 406 (1986).
[25] S. P. Sander, D. M. Golden, M. J. Kurylo, V. L. Orkin, A. R. Ravishankara, R. R. Friedl, C. E. Kolb, M. J. Molina, G. K. Moortgat, B. J. Finlayson-Pitts, and R. E. Huie, *Chemical Kinetics and Photochemical Data for Use in Stratospheric Modeling*, NASA: JPL Publication 02-25, CA (2003).
[26] J. R. Alvarez-Idaboy, N. Mora-Diez, R. J. Boyd, and A. Vivier-Bunge, J. Am. Chem. Soc. **123**, 2018 (2001).
[27] V. H. Uc, I. García-Cruz, A. Hernández-Laguna, and A. Vivier-Bunge, J. Phys. Chem. A **104**, 7847 (2000).
[28] (a) WMO Global Ozone Research and Monitoring Project, *The Stratosphere 1981: Theory and Measurements*, Rep. 11 (1982).
(b) R. J. Cicerone, S. Walters, and S. C. Liu, J. Geophys. Res. **88**, 3647 (1983).
[29] W. S. Xia and M. C. Lin, J. Chem. Phys. **114**, 4522 (2001).

DOI:10.1088/1674-0068/21/01/32-38